Spring 5-5-2011

CFD Modeling of Fluidized Bed Reactor for the Synthesis of Dimethyl Ether

Ranjeeth Kalluri
RTI International

Nandita Akunuri
RTI International

aqil Jamal
RTI International

Raghubir Gupta
RTI International

CFD MODELING OF FLUIDIZED-BED REACTOR FOR THE SYNTHESIS OF DIMETHYL ETHER

Ranjeeth Kalluri, Nandita Akunuri, Aqil Jamal, and Raghubir Gupta
RTI International, P.O. Box 12194, Research Triangle Park, NC 27709-2194, USA

ABSTRACT

The syngas-to-DME reaction is highly exothermic, and the catalyst temperature window is very narrow. The fluidized-bed reactor is, therefore, an ideal choice to carry out these reactions. RTI is developing a circulating fluidized bed design for DME synthesis. This paper discusses a two-phase CFD model and optimization of the solids circulation rate.

INTRODUCTION

In recent years, dimethyl ether (DME) has been generating broad interest as a promising alternative transportation fuel with great potential impact on society. DME is also a key chemical intermediate in the production of several petrochemicals such as dimethyl sulfate, synthetic gasoline, polymer-grade ethylene and propylene, and acetonitrile, a solvent used in the battery industry. Production of DME worldwide has increased from 30,000 tonnes/yr in 2000 to 545,000 tonnes/yr in 2006, and is expected to continue to rise over the next decade, due to the planned construction of multiple DME production facilities, especially in Asia(1). The conventional production of DME utilizes carbon monoxide (CO) from syngas. The recent recognition of DME synthesis from carbon dioxide (CO_2) as a potential means to mitigate global CO_2 emissions has further added to the growing interest in DME research.

Commercially, DME is produced in a two-step process, where syngas is first converted to methanol, and the methanol produced is dehydrated to DME. This process mainly involves the following three reactions:

Methanol synthesis reaction: $CO + 2H_2 \leftrightarrow CH_3OH \qquad \Delta H = -98.744\ \text{kJ/mol}$ (1)

Water gas shift reaction: $CO + H_2O \leftrightarrow CO_2 + H_2 \qquad \Delta H = -21.255\ \text{kJ/mol}$ (2)

Methanol dehydration reaction: $2CH_3OH \leftrightarrow CH_3OCH_3 + H_2O \qquad \Delta H = -40.9\ \text{kJ/mol}$ (3)

Reactions (1) and (2) are catalyzed by a methanol synthesis catalyst ($Cu/ZnO/Al_2O_3$) and reaction (3) is catalyzed by an acid catalyst. All the above three reactions are reversible and exothermic, which results in a narrow catalyst operating temperature window. Combining the above reactions so that they occur simultaneously allows inhibiting products from one equilibrium reaction to be consumed in another, creating a strong driving force for the production of DME(2). The methanol produced in

reaction (1) is consumed by reaction (3), and the water (H_2O) formed in reaction (3) is consumed in reaction (2), thereby driving reaction (3), and producing additional hydrogen (H_2) required for the methanol production (reaction (1)). The net reaction for the direct syngas-to-DME process can be given as:

Overall Reaction: $3CO + 3H_2 \leftrightarrow CH_3OCH_3 + CO_2 \qquad \Delta H = -256.615\,\text{kJ/mol}$ (4)

Numerous commercial DME production processes are available from companies such as Haldor Topsoe, Lurgi, Mitsubishi Gas Chemical, etc. However, most of these designs are two-step processes that are extensions of existing methanol synthesis facilities, and are not optimized for the production of DME. Recent developments for direct syngas-to-DME (single-stage) production include the use of slurry phase reactors such as that employed by JFE Holdings, Inc., Japan (3). Although the slurry-phase reactor provides improved conversion efficiency due to efficient removal of the heat generated by reactions (1) - (3), the product recovery at typical operating conditions requires cryogenic separation (< 213 K).

An alternative reactor design for direct DME synthesis is a fluidized-bed reactor. Lu *et al.* (4) have demonstrated experimentally that the per-pass CO conversion can be significantly improved using two-phase fluidized-bed reactors compared to slurry reactors. These authors have also shown the DME selectivity to be notably higher in fluidized-bed reactors compared to slurry reactors. Fluidized-bed reactors offer higher gas-solid mass transfer rates, which lead to higher DME yields compared to slurry reactors. Dynamic mixing of particles in a fluidized-bed also eliminates hot spot formation. Elimination of hot spots is critical for an extended catalyst life time (5), as the catalyst rapidly deactivates at higher temperatures (> 570 K). Further, at higher temperatures the equilibrium does not favor a high DME yield. These catalyst deactivation and equilibrium restrictions lead to a narrow catalyst operating temperature window.

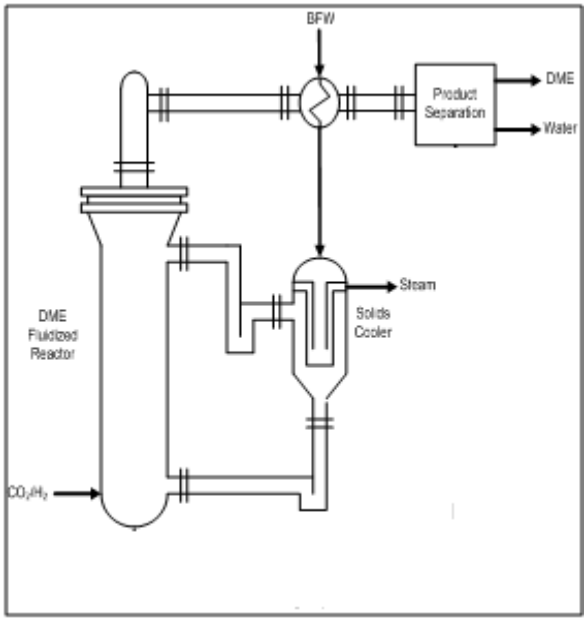

Figure 1: Schematic of the CFB design

Effective temperature control in a fluidized-bed reactor can be achieved by circulating boiler feed water through internal coils within the reactor. The major challenge for this internal cooling scheme is the design of the reactor internals, which provide maximum heat recovery. To overcome these limitations, RTI is exploring a circulating fluidized-bed (CFB) reactor design with an external solids-cooler. In this approach, the catalyst is circulated between the fluidized-bed reactor and an external solids-cooler, where the solids act as a heat transport medium to carry heat out of the reactor, thereby allowing for control of the reactor temperature. A schematic of this process is shown in Figure 1. This process ensures high

heat transfer rates and applicability of commercial solid cooling systems typically used in fluid catalytic cracking (FCC) processes.

In this paper, a computational fluid dynamics (CFD) model for simulating the two phase (gas-solid) fluidized-bed DME synthesis process was developed using Fluent 12.1. The model developed was first validated with the experimental fluidized-bed results obtained by Lu *et al*. (4). This validated model was then used to study the benefits of a CFB reactor with external solids cooling for DME synthesis, and to optimize the solids circulation rate for maximizing CO conversion and DME yields. This CFD model can be further used for design and scale-up of the proposed CFB reactor for DME production.

CFD MODEL

The two different fluidized-bed geometries (described in detail in the next section) considered in this study were modeled using 2-D axisymmetric models using Ansys Fluent 12.1. The Eulerian-Eulerian approach has been used to model the fluid-solid flow dynamics. This model considers both the primary and the secondary (dispersed) phases to be interpenetrating continua. The equations considered (6) in the model are summarized below.

The generalized continuity equation can be written as (*i*= *g* or s):

$$\frac{\partial(\rho_i \varepsilon_i)}{\partial t} + \nabla \cdot (\rho_i \varepsilon_i \vec{v}_i) = 0 \tag{5}$$

The momentum balance equations for gas and solid phases can be written as (*i, k* = *g* or *s*):

$$\frac{\partial(\rho_i \varepsilon_i \vec{v}_i)}{\partial t} + \nabla.(\rho_i \varepsilon_i \vec{v}_i \vec{v}_i) = \rho_i \varepsilon_i \vec{g} - \varepsilon_i \nabla P + \nabla.\bar{\bar{\tau}}_i + \beta(\vec{v}_k - \vec{v}_i) \tag{6}$$

The generalized energy conservation equation for the gas and solid phases is:

$$\frac{\partial(\rho_i \varepsilon_i H_i)}{\partial t} + \nabla.(\rho_i \varepsilon_i u_i H_i) = \nabla(k_i \nabla T_i) + h_{ki}(T_k - T_i) \tag{7}$$

For the solid phase, the random granular motion resulting from particle collision is described by the following transport equation:

$$\frac{3}{2}\left[\frac{\partial(\rho_s \varepsilon_s \Theta)}{\partial t} + \nabla(\rho_s \varepsilon_s \Theta \vec{v}_s)\right] = (-P_s \bar{\bar{I}} + \bar{\bar{\tau}}_s) : \nabla \vec{v}_s + \nabla.(\kappa_s \nabla \Theta) - \gamma + \phi_{gs} \tag{8}$$

where the first term on the right hand side is the generation of energy by the solid stress tensor, the second term denotes the diffusion of energy, the third term represents the collisional dissipation of energy, and the fourth term represents the energy exchange between the solid and the gas phase.

The generalized conservation equation for the various species in the gas phase is:

$$\frac{\partial}{\partial t}\left(\rho_g \varepsilon_g Y_{g,j}\right) + \nabla\left(\rho_g \varepsilon_g \vec{v}_g Y_{g,j}\right) = -\nabla.\varepsilon_g J_{g,j} + R_j \quad (9)$$

The rate expressions and parameters from Lu *et al.* (7) were used to model the reactions involved in the DME synthesis process. The activity of the catalyst was assumed to remain constant, with no deactivation occurring with time. The rate expressions used for the three individual reactions (1) - (3), are:

$$r_1 = \frac{k_1 K_{CO}\left[p_{CO} p_{H_2}^{3/2} - p_M / (p_{H_2}^{0.5} K_{P_1}^0\right]}{\left(1 + K_{CO} p_{CO} + K_{CO_2} p_{CO_2}\right)\left[p_{H_2}^{0.5} + \left(K_W / K_{H_2}^{0.5}\right) p_W\right]} \quad (10)$$

$$r_2 = \frac{k_2 K_{CO_2}\left[p_{CO} p_W - \left(p_{CO_2} p_{H_2} / K_{P_3}^0\right)\right]}{\left(1 + K_{CO} p_{CO} + K_{CO_2} p_{CO_2}\right)\left[p_{H_2}^{0.5} + \left(K_W / K_{H_2}^{0.5}\right) p_W\right]} \quad (11)$$

$$r_3 = \frac{k_3\left[p_M - \left(p_D p_W / K_{P_2}^0\right)^{0.5}\right]}{\left[1 + K_M\left(p_D p_W / K_{P_2}^0\right)^{0.5}\right]^2} \quad (12)$$

As will be further discussed in the next section, these kinetic rate expressions were validated against experimental data reported by Lu *et al.* (4). While the methanol synthesis catalysts used in both these studies (4 and 7) were similar (Cu-ZnO-Al_2O_3), the methanol dehydration catalyst was different, γ-alumina by Lu *et al.* (4) and HZSM-5 by Lu *et al*. (7). In view of this difference in the methanol dehydration catalyst used, kinetic constant k_3 was varied to enable a better fit of the CFD model with the experimental results, while all the other rate and equilibrium constants used in the above rate expressions were left unchanged from those published by Lu *et al*. (7). An order-of-magnitude-lower value for the pre-exponential factor for k_3, compared to that reported by Lu *et al*. (7), yielded a better fit of the CFD data with the experimental results, and hence it was used for this entire study. For the purpose of this study, the CO conversion and DME selectivity was defined as:

$$X_{CO} = \frac{(N_{CO})_{in} - (N_{CO})_{out}}{(N_{CO})_{in}} \quad (13)$$

$$S_{DME} = \frac{2N_{DME}}{2N_{DME} + N_{MeOH}} \quad (14)$$

$$P_{DME} = \frac{M_{DME}}{M_{cat}} \quad (15)$$

CFD SIMULATIONS AND RESULTS

Validation of the CFD Model

As described above, the CFD model was first validated with the experimental CO conversion results obtained by Lu *et al.* (4). The reactor geometry and operating conditions used in this published experimental study are summarized in Table 1. Also shown in the table are the assumed catalyst thermal properties (conductivity and specific heat), which correspond to the alumina (catalyst support). A particle

sphericity of 0.8 was assumed in this study to account for the particle surface roughness. The experimental study by Lu *et al.* was conducted over a pressure range of 2 MPa to 4 MPa and a H_2/CO ratio of 0.8 to 2.1. A fixed gas space velocity of 3000 ml/g cat/h (STP) was used in all these experimental tests.

Transient CFD cases representing each of these experiments were simulated. An isothermal wall boundary condition (533 K) was used in all these simulations to simulate the experimental conditions. Each of the simulations was run for at least three (gas) residence times, so as to obtain steady state outputs. The output composition and flow rate were monitored and plotted**.** Figure 2 shows the typical outlet mole fractions and flow rate variations with flow time as predicted by the CFD simulation. The outlet gas composition and flow rate typically approached relatively constant values in about one (gas) residence time from startup. Other process variables such as temperature and pressure also showed similar stabilization patterns. To eliminate the effect of small fluctuations present in these output flow variables, time-averaged (10 s) values were used in assessing the steady-state performance of the reactor.

Figure 3 shows the axial profiles of solids volume fraction, and mole fractions of CO, H_2, and DME for the case of inlet H_2/CO ratio of 1.0 and 3 MPa reactor pressure. For these conditions, the bed expanded to about 1.40 m in height. The solids fraction increased gradually along the length of the reactor, as the gas volume (molar) flow decreased due to the reactions. The concentrations of CO and H_2 decreased, as they were consumed by the reactions, and methanol and DME concentrations increased along the

Table 1: Operating conditions and parameters

Reactor diameter (m)	0.026
Reactor length (m)	2.0
Bed height at min. fluidization (m)	1.0
Inlet & wall temperatures (K)	533
Packed bed voidage	0.428
Catalyst particle diameter (μm)	150
Catalyst sphericity	0.8
Catalyst density (kg/m^3)	1983
Catalyst specific heat (J/kg K)	880
Catalyst thermal conductivity (W/m.K)	35

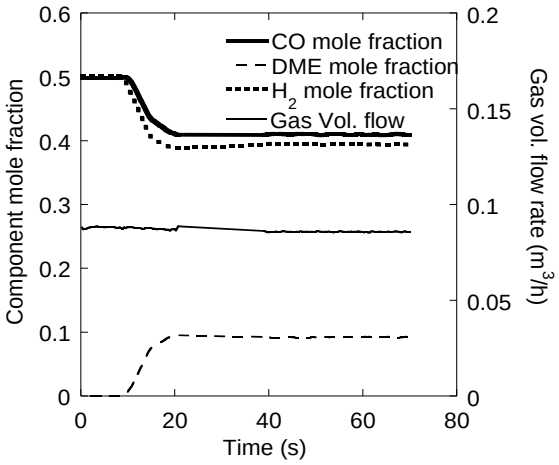

Figure 2: Outlet stream composition and flow rate variation with time (P=3 MPa, H_2/CO=1.0, T=533 K, and SV=3000 ml/gcat/h)

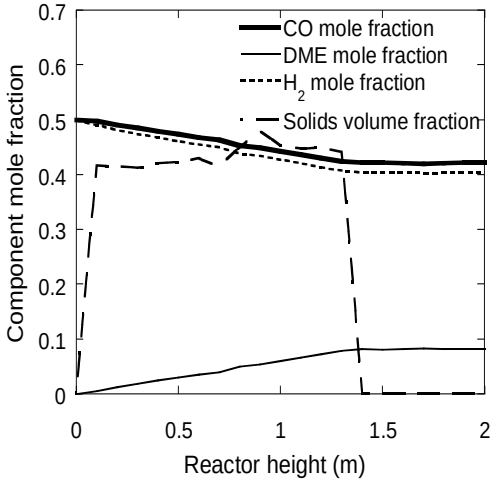

Figure 3: Profile plots of component compositions and solid volume fractions at t=70 s (P=3 MPa, H_2/CO=1.0, T=533 K, and SV=3000 ml/gcat/h)

length of the reactor. Similar patterns were seen for the other reactor pressures and H_2/CO ratios studied. The maximum temperature rise in any of these cases was less than 5 K, due to the isothermal wall boundary conditions and small reactor diameter used. The mole fraction of water (not shown in the figure) remained low (< 0.01) throughout the reactor, as the water gas shift reaction consumed most of the water generated by the methanol synthesis and methanol dehydration reactions.

Figure 4 and Figure 5 show a comparison of CFD and experimental (4) results of CO conversion as a function of inlet gas composition and pressure, respectively. The CO conversion values are in good agreement with the experimental results for the entire range of pressure and H_2/CO ratios reported by Lu *et al*. (4). The figures also show DME selectivity and productivity for various inlet conditions. For the same gas space velocity, increase in H_2/CO ratio led to higher CO conversion (Figure 4), as the methanol synthesis reaction has higher (order) dependence on H_2 partial pressure (1.5) than on CO partial pressure (1.0). Also, an increase in pressure led to higher conversions and DME productivities (Figure 5), due to higher reactant partial pressures and effective gas residence times in the reactor. The DME selectivity decreased with increasing conversions, as the increasing DME concentrations deterred the methanol dehydration (equilibrium) reaction.

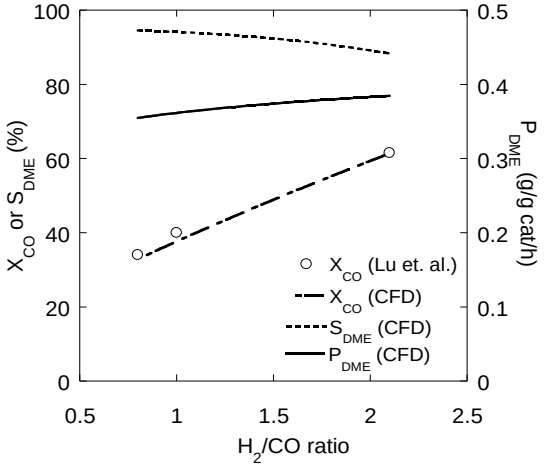

Figure 4: Effect of feed composition on simulation and experimental results (P=3 MPa, T=533 K, and SV=3000 ml/gcat/h)

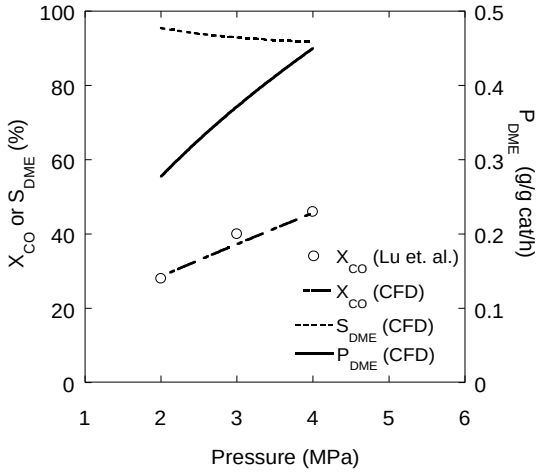

Figure 5: Effect of pressure on simulation and experimental results (H_2/CO=1.0, T=533 K, and SV=3000 ml/gcat/h)

Circulating Fluidized-bed Optimization

Lu *et al*. (4) demonstrated through experimental results that the optimum reactor temperature for maximizing CO conversion and DME yield lies in the range of 550 K to 570 K, for an inlet gas pressure of 3 MPa and H_2/CO ratio of 1.0. The kinetics of methanol synthesis are limiting at lower temperatures, whereas the equilibrium restricts CO conversion at higher temperature. This leads to a narrow temperature window for optimal reactor operation and hence makes the ability to attain precise temperature control in the reactor critical. As described previously, in this study, benefits of using a CFB reactor with an external solids cooling loop (Figure 1) for effective temperature control in the DME synthesis process were explored.

A series of CFD simulations were conducted using the above validated CFD model on a modified fluidized-bed geometry to optimize the solids circulation rates for maximizing CO conversion and DME yield. The circulating fluidized-bed geometry used for this study had a length of 4.0 m and a diameter of 0.026 m. In these simulations, feed gas and catalyst particles entered the reactor at 533 K and 3 MPa. The feed gas flow rate was fixed at 90 SLPM, and the solids/gas ratio entering the reactor was varied between 10 and 30, by changing the solids mass flow rate entering the reactor. The reactor wall boundary condition in these simulations was set to the adiabatic (no heat flux) condition. All the exothermic heat released from the reactions was carried out of the reactor exclusively by the catalyst particles and product gases exiting the reactor. The catalyst, thereby, served dual functions – reaction rate promoter as well as heat transport medium. Further, the hot solids exiting the reactor were assumed to be separated and cooled to 533 K, before being recirculated to the reactor.

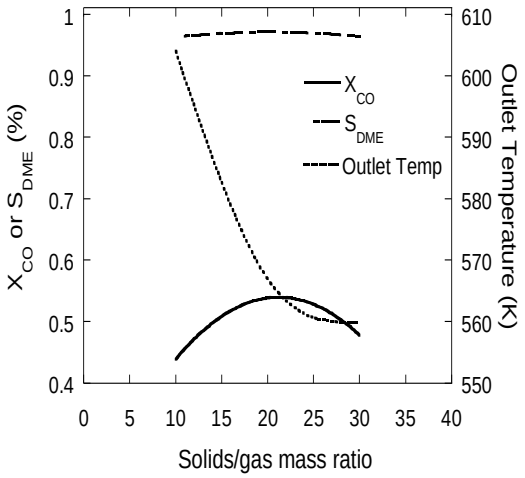

Figure 6: Effect of inlet solids/gas mass ratio on performance of CFB reactor for DME production (Inlet conditions: P=3 MPa, T=533 K. and H_2/CO=1.0)

Figure 6 shows the effect of inlet solids/gas mass ratio on CFB reactor performance. For maximum CO conversion, the optimum solids/gas ratio appears to be around 20. As expected, with increase in solids/gas mass ratio, the outlet temperature decreased significantly, as the increasing solids flow absorbs more heat. The optimum solids/gas ratio (=20) for CO conversion also corresponds with the outlet temperature of 565 K, which is in the optimum reactor operating temperature range suggested by Lu *et al*. (4). A lower (<20) solid/gas ratio leads to excess reactor temperature, resulting in equilibrium limitations, whereas a higher (>20) solid/gas ratio leads to low reactor temperatures and kinetic limitations.

CONCLUSIONS

The CFD model developed in this study was successfully validated with experimental DME synthesis fluidized-bed results from the literature. It was further used to demonstrate the benefits of using a CFB reactor with external solids-cooler to control the bed temperature. The model predicted an optimal solids/gas ratio for highest CO conversion and/or DME yield to be about 20 for the catalyst (kinetics) used in this study. In this concept, the catalyst particles act as a heat sink to carry heat out of the reactor, apart from catalyzing the DME synthesis reactions. The kinetic model used in this analysis was validated using literature data. Further validation of the CFD model using our own experimental data is under way.

NOTATION

g acceleration due to gravity (m/s^2)
h_{sg} heat transfer coefficient ($W/m^2.K$)
H enthalpy (J/kg)
$J_{g,j}$ diffusion flux (kg/m^2s)
k rxn rate constant (units vary)
K reaction equilibrium constant
M_{cat} mass of catalyst in reactor (g)
M_{DME} DME outlet mass flow rate (g/h)
N_{CO} molar flow rate of CO (mol/s)
N_{DME} molar flow rate of DME (mol/s)
N_{MeOH} molar flow rate of CH_3OH(mol/s)
p partial pressure of species 'j'
P pressure (bar)
P_{DME} productivity of DME (g/g(cat)/h)
S_{DME} selectivity of DME in products, dimensionless
T temperature (K)
r reaction rate, mol/gcat/s
R_j rate of production of species 'j'
$\vec{v}_i$ mean velocity of the phase (m/s)
X_{CO} conversion of CO, dimensionless

Greek Letters

β drag coefficient ($kg/m^3.s$)
ε dense phase voidage, dimensionless
κ_s energy diffusion coefficient
ρ density, kg/m^3
τ stress tensor (bar)
ϕ_{gs} energy exchange between gas and solid phase
Θ granular temperature
γ dissipation of fluctuating energy (W/m^3)

Subscripts

i gas or solid phase
k interacting phase
j species 'j'
g gas phase
s solid phase

REFERENCES

1. Reuters. (2008). "China domestic production of dimethyl ether is expected to reach 4.36 million tons in 2008." [cited 2009 Aug. 26]; Available from: http://www.reuters.com/article/pressRelease/idUS140041+08-Aug-2008+BW20080808
2. Wang, Z., Wang, J., Diao, J., and Jin, Y. (2001). "The synergy effect of process coupling for dimethyl ether." *Chem. Eng. Tech.*, 24, 507-511.
3. Bourg, H. M. (2006). "Future Prospective of DME." *23rd World Gas Conference*, Amsterdam.
4. Lu, W., Teng, L., and Xiao, W. (2004). "Simulation and experiment study of dimethyl ether synthesis from syngas in a fluidized-bed reactor." *Chem. Eng. Sci.*, 59, 5455-5464.
5. Cooper, M., (2010). "Direct synthesis of dimethyl ether from syngas using a novel fluidizable catalyst." *Internal R & D Report,* RTI International, Durham, NC.
6. Ansys Inc. "Ansys *Fluent Theory Guide* - Ansys Fluent 12.0."
7. Lu, W.Z., Teng, L.H., and Xiao, W.D. (2003). "Theoretical analysis of fluidized-bed reactor for dimethyl ether synthesis from syngas." *Intl. J. of Chem. Reactor Eng.*, 1, S2.